Brownfield TDM-PON and Clustering Assisted 5G-3D beamforming Based Cost-Efficient FiWi Access Network Deployment

Nilesh Chatur, Tushar Bose, and Aneek Adhya, *Member, IEEE,*

***Abstract*—In recent times, usage of fixed wireless access (FWA) is gaining momentum even though fiber based existing services such as fiber-to-the-home (FTTH) are widely used for home Internet applications. We explore a time-division multiplexing passive optical network (TDM-PON) and long term evolution advanced (LTE-A) based cost-efficient access network planning strategy for combined usage of FWA and FTTH with the same network infrastructure. The proposed fiber-wireless (FiWi) access network satisfies all feasibility constraints and users' quality of service (QoS) requirements. The proposed planning method judiciously identifies the network architecture and user service mode (FWA/FTTH).**

***Index Terms*—Fiber-wireless (FiWi), fixed wireless access (FWA), passive optical network (PON), 5G.**

I. Introduction

WITH the introduction of fifth-generation (5G) technology, fixed wireless access (FWA) has become an attractive use case. The ease of depolyment coupled with cost efficiency makes FWA a promising solution to deliver high-speed network services at remote locations. Furthermore, FWA is used to provide network services to users in situations where wired infrastructure is either unavailable or prohibitively expensive to deploy. Therefore, FWA has become a popular choice for telecom operators such as Verizon and AT&T [1], [2]. 5G millimeter-wave (mmW) technology is one of the key enablers for FWA due huge bandwidth availability and low latency connectivity over short distances. However, mmWave is easily blocked by obstacles such as buildings and trees and have high propagation losses. These aforementioned propagation challenges can be mitigated in mm-wave bands through beamforming.

Beamforming is a signal processing technique that is used to transmit and receive signals in a desired direction [3]. Beamforming leads to the reduction of interference and noise in the network by transmitting signals to the intended users only. Beamforming is achieved by utilizing multiple antennas at the transceiver. Furthermore, in a multi-user scenario, beamforming enhances the signal-to-noise (SNR) at the receiver by cancelling the co-channel interference [4]. The short wavelength of mmW band facilitates the fabrication of on-chip antenna elements with high packaging density without increasing the form factor of the base station (BS). Antenna-in-package (AiP) [5] is a popular technology utilized in mmW bands to fabricate multiple antenna elements on a single chip. These antenna elements are used to form high-gain directional beams, in accordance with the third-generation partnership project (3GPP) standards of 5G. Apart from conventional time and frequency resources, beamforming also utilizes spatial directions. Multiple concurrent beams transmitted from the next generation Node B (gNB) are used to serve users in different directions simultaneously, thereby improving the spatial multiplexing gain. Multiple beams generated by the antenna array are directed in different directions by controlling the amplitude and phase of the individual antenna elements. The aforementioned advantages of beamforming in the mmW frequency bands motivate us to employ 3D beamforming to provide network services to the users associated with the wireless gNBs in the FWA network. FWA utilizes optical fiber for backhaul and wireless coverage for the front-end, connecting the BS to the customer premises equipment (CPE) [2].

It is anticipated that the digital divide between rural, sub-urban, and urban areas can be effectively reduced by using a combination of Fixed Wireless Access (FWA) and Fiber-to-the-Home (FTTH) based access networks. This combination can be achieved effectively through the implementation of hybrid Fiber-Wireless (FiWi) access networks. FiWi integrates a fiber-based passive optical network (PON) and a wireless access network, such as a wireless mesh network, Long Term Evolution (LTE)/LTE Advanced (LTE-A), and 5G, or a combination of these technologies [6]–[8]. However, inefficient deployment FiWi access network results in degraded quality of service (QoS) and increased capital expenditure (CapEx). To address the aforementioned challenges in FiWi deployment, in this paper we explore topology optimization for FiWi access networks. We consider the combined usage of multistage time-division multiplexing PON (TDM-PON) and 5G mmW technology. The TDM-PON and 5G networks operate independently and are integrated through a radio-and-fiber (R&F) enabling method [9]. The users can receive a fiber connection using FTTH through an optical network unit (ONU), or a wireless connection using FWA through a CPE at their residence (Fig. 1).

Most of the current research works do not cater to the OFDMA-based resource allocation in 5G adequately. Therefore, in this paper, we enhance physical resource utilization by considering a 3-dimensional (3D) resource grid. The 3D

The authors are with the G. S. Sanyal School of Telecommunication, Indian Institute of Technology (IIT) Kharagpur, Kharagpur 721302, India (e-mail: nileshchatur@iitkgp.ac.in; btushar@kgpian.iitkgp.ac.in; aneek@gssst.iitkgp.ac.in).

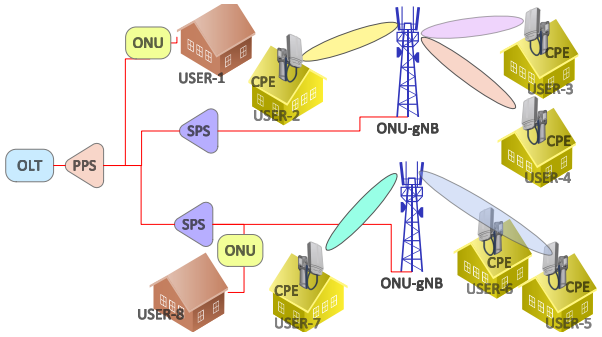

Fig. 1: Multistage TDM-PON and 5G based FiWi network architecture.

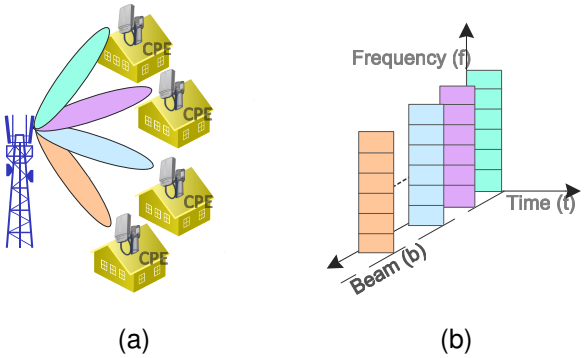

Fig. 2: (a) Beamforming at BS (b) BFT RB grid.

resource grid is presented in Fig. 2. In the 3D resource grid, resource utilization is enhanced by considering multiple beams as physical resource elements coupled with the time-frequency resource block (RB).

Beam assignment to the users in 5G new radio (NR) is achieved through the initial access process [10]. The beam assignment is the process of selecting the most appropriate beam for the user based on various parameters (viz., signal quality, channel conditions, and interference levels). The gNB steers beams to send the Synchronization Signal Block (SSB) to all users present over the geographical area of interest. The users evaluate the received signal quality of different SSBs transmitted over the different beams and report the best beam index to the gNB. The beam management process is a four steps procedure for both uplink and downlink transmission in 5G NR [10], [11]. With respect to beam management, in this paper, we consider the downlink procedure (i.e. transmission from gNB to the user). The first step is beam sweeping, in which the gNB uses a set of predetermined beams to transmit SSB to cover the given geographical area of interest. In the second step, the user performs beam measurement by evaluating the quality of the received signal. The evaluation of the received signal is done through various performance metrics such as Reference Signal Received Power (RSRP), and Received Signal Strength Indicator (RSSI) [10]. In this paper, we utilize RSRP as the metric to characterize the quality of the received signal. In the third step, the user performs the beam determination by selecting the appropriate beam or beams based on the RSRP measurements. In the fourth step of beam reporting, users send the beam decision based on beam measurement to the gNB.

The users to be connected to OFDM-based wireless networks are limited by the number of RBs and beams available at gNB, the channel condition experienced by the users, and users' data rate demand. Further, users to be connected by fiber are restricted by the splitting ratio of the power splitter (PS), line rate of fiber, and users' data rate demand. In case both the wireless and fiber-based service modes (i.e., FWA and FTTH) satisfy the users' QoS, the users are preferred to be connected through wireless (i.e., FWA) mode due to cost efficiency. However, due to limited resource (i.e., RB, beams, and transmission power) availability at BSs, all users cannot be accommodated through the wireless mode. Thus, network architecture and user connection mode (fiber/wireless) are required to be optimally identified.

II. Contributions

.

In this paper, we propose a cost-efficient TDM-PON and 5G-based Fi-Wi user-centric access network to provide network services over a given geographical area of interest. The proposed framework computes the optimal (minimal) CAPEX of the network deployment such that the desired QoS constraints for each user are satisfied in the network. The main contributions of this work are summarized below

- Keeping in view the network CAPEX, we compute the optimal number of gNBs constrained by the total number of gNBs available with the telecom network operator. To compute the optimal number of gNBs, we partition the users present in the given geographical area of interest into disjoint clusters. We utilize the location information of the users to obtain disjoint clusters by employing the framework of unsupervised machine learning (ML). Furthermore, utilizing the location information, we also determine the optimal locations of the gNBs in the geographical area.
- Next, we derive a beam code book with a uniform planar array (UPA) installed at the gNBs to steer high-gain beams in different directions so as to cover the effective service radius of the gNB. We derive the beamforming vector for the simultaneous beam generation by the UPA installed at gNB.
- We utilize a realistic cluster-based mmW channel model to compute the RSRP for each wireless user. Moreover, the closed-form expression utilized for RSRP computation accounts for path-loss (PL), shadowing, line of sight (LoS) probability of the users, antenna gains, and the small-scale fading effects.
- We propose an integer linear programming (LP) based optimization framework to determine the user association to the wireless network (i.e., through gNBs) or to the fiber-based (TDM-PON) network. The proposed optimization framework minimizes the network CAPEX and it also ensures that the desired QoS constraint is satisfied for all the users in a user-centric 5G FiWi access network. Furthermore, the proposed optimization

framework also determines wireless resource allocation from the 3D resource grid (i.e. optimal beam and RB).
- We perform extensive simulations to demonstrate the effectiveness of our proposed framework of a user-centric 5G FiWi access network. The simulation results are illustrated for various 5G outdoor deployment scenarios of 3GPP standards such as rural macro (RMa), urban macro (UMa), and urban micro (UMi) street canyon.

III. Related Works

IV. Organization of the Paper

The rest of the paper is organized as follows. Section V describes the system model of this work followed by problem formulations.

V. System Model and Problem Formulations

This section discusses the system model and problem formulations. In the first subsection, we present the system model of this work. The next subsection discusses the problem formulations. The first problem relates to the partitioning of users into disjoint clusters. The disjoint clusters are characterized by their respective cluster centers or centroids. The first problem also deals with identifying the optimal location of the cluster centroids and the computation of the optimal number of gNBs constrained by a maximum number of gNBs available with the telecom network operator. The second problem relates to the association of users with the gNB (wireless) or with the TDM-PON infrastructure so as to minimize CAPEX. The CAPEX is minimized such that the desired QoS constraints are satisfied for all the users present in the network spanned over a given geographical area. Furthermore, the second problem also performs the optimal resource allocation (ie.e beam and RBs) from the 3D resource grid.

A. System Model

The system model of this work is presented in Fig. 1. fig desription. We implement a network planning problem where the users are distributed over a given geographical area (A) and need to be provided with network coverage. The network services are provided optimally to the users either through gNBs (wireless) or by using the fixed infrastructure of TDM-PON so as to simultaneously reduce the CapEx and satisfy the desired QoS requirement. The set of users is denoted by $U = \begin{Bmatrix} u_1 & u_2 & \cdots & u_i & \cdots & u_{N_u} \end{Bmatrix}$. The total number of users in A is N_u. Without the loss of generality, we consider that the users are deployed on the x-y plane. It is assumed that the location of the users is known apriori. This assumption is valid as the location information can be easily obtained by using a global positioning system (GPS). The x and y coordinates of i^{th} user (i.e., u_i) is represented by, $u_i = \{u_{ix}, u_{iy}\}, i = 1, 2, \cdots, N_u$. The location of the users is stored in a matrix U^l expressed as

$$U^l = \begin{bmatrix} u_{1x} & u_{1y} \\ u_{2x} & u_{2y} \\ \cdots & \cdots \\ u_{ix} & u_{iy} \\ \cdots & \cdots \\ u_{N_u x} & u_{N_u y} \end{bmatrix}_{N_u \times 2} . \quad (1)$$

U^l is a $N_u \times 2$ matrix where the i^{th} row represents the user u_i. The first and second columns of U^l represent the user u_i's x and y coordinates, respectively. In view of a CAPEX-constrained network design, we consider that the geographical area (A) is divided into $|C|$ disjoint clusters. The set of clusters is given as $C = \begin{Bmatrix} c_1, & c_2, & \cdots & c_c, & \cdots, & c_{N_c} \end{Bmatrix}$, and $|C|$ represents the cardinality of set C (i.e., number of elements in set C is N_c). The maximum number of gNBs available with the network operator is N_g. The set of gNBs is given as $G = \begin{Bmatrix} g_1 & g_2 & \cdots & g_j & \cdots & g_{N_g} \end{Bmatrix}$.

We consider that each gNB (g_j) is equipped with three UPAs. Each UPA (of gNB g_j) is capable of generating a total of N_b simultaneous beam. Thus, each gNB is capable of transmitting $3N_b$ simultaneous beams (for three sectors). The designed beam codebook vector i.e., the set of beams generated by each gNB (g_j) is expressed as $B^j_{des} = \begin{Bmatrix} b^j_1, & b^j_2, & \cdots, & b^j_k, & \cdots, & b^j_{3N_b} \end{Bmatrix}$. The complete designed codebook tensor (i.e. $B^j_{des} \forall j = 1, 2, \cdots, N_g$) for network spanned over geographical area A is given as,

$$B^{CD} = \begin{bmatrix} b^1_1 & b^1_2 & \cdots & b^1_k & \cdots & b^1_{3N_b} \\ b^2_1 & b^2_2 & \cdots & b^2_k & \cdots & b^2_{3N_b} \\ \cdots & \cdots & & & & \\ b^j_1 & b^j_2 & \cdots & b^j_k & \cdots & b^g_{3N_b} \\ \cdots & \cdots & & & & \\ b^{N_g}_1 & b^{N_g}_2 & \cdots & b^{N_g}_k & \cdots & b^{N_g}_{3N_b} \end{bmatrix}_{N_g \times 3N_b} . \quad (2)$$

The k^{th} beam of j^{th} gNB (i.e b^j_k) can be steered to the desired direction (i.e., at a given azimuth and elevation angle) by designing a suitable beamforming vector. For simplicity, we consider that the user devices are equipped with a single antenna. However, our proposed framework can be easily extended for users equipped with multiple antennas (viz., uniform linear array (ULA), UPA) or other existing antenna array geometries.

We consider that Z is the set of RBs (time and frequency slots) available at each beam of a given gNB (i.e., b^j_k), and M is the set of available MCS classes. Further, $z, z \in Z$ represents a particular resource element in Z. Therefore, each physical resource element of 3D resource grid is defined as $R_{3d} = \left(b^k_j, z\right)$

B. Problem Formulations

The problem formulation to obtain disjoint cluster of users, the optimal number of gNBs, and optimal coordinates for cluster centroids utilizing the location information of users are stated as problem P1.

$$\text{P1: } C^* = c^* = \arg\min_{c} \left(\sum_{c \in C} \sum_{i \in U} \|D_{c,i} - \mu_c\|^2 \right) \quad (3)$$

Subject to,

$$C_c \bigcap_{c,\bar{c}=1,c\neq\bar{c}}^{N_c} C_{\bar{c}} = \Theta \tag{4a}$$

$$\sum_{c\in C} \tilde{u}_{i,c} = 1 \quad \forall i \in U \tag{4b}$$

$$C_c \bigcup_{c,\bar{c}=1,c\neq\bar{c}}^{N_c} C_{\bar{c}} = A \tag{4c}$$

$$\sum_{c\in C} C_c \leq N_g \tag{4d}$$

The objective function of P1 in equation 3 is to compute the optimal number of clusters (C^*) by minimizing the sum of squared distances between the user and cluster centers. The computed optimal number of clusters also results in obtaining the optimal number of gNBs. Furthermore, the obtained optimal coordinates of the cluster centroids also represent the location of the gNB (i.e., a gNB consisting of three UPAs, each UPA serving one sector). Constraint in equation 4a guarantees that the intersection of two disjoint clusters of users over the considered geographical area A results in a null set Θ. The constraint in equation 4b indicates that a user is associated with only one unique cluster. In equation 4b $\tilde{u}_{i,c}$ is a binary variable such that ($\tilde{u}_{i,c} = 1$ if user i is associated with cluster c; 0 otherwise.)
Constraint in equation 4c ensures that the union of all clusters $C = \{C_1, C_2, \ldots, C_{N_c}\}$ cover the entire geographical area of interest A. In the interest of CAPEX-constrained network design, constraint in equation 4d guarantees that the optimal number of disjoint clusters obtained is less than or equal to the maximum number of gNBs (N_g) available to the network operator.

Utilizing the framework of the problems (P1), we obtain the disjoint cluster of users, the optimal location of the cluster centers, and the optimal number of gNBs. Next, we propose the ILP-based optimization framework (i.e. Problem P2) to obtain the optimal user association to the wireless (i.e. gNBs) or to the wired (i.e. TDM-PON) access network. Furthermore, the proposed optimization framework utilizes a minimum spanning tree (MST) algorithm to obtain the minimum CAPEX for the overall optimized network. The user association obtained utilizing the proposed minimum CAPEX optimization framework ensures minimum deployment cost for a user-centric 5G FiWi network. The proposed ILP-based optimization framework also ensures that the desired QoS requirements are satisfied for all users distributed over the geographical area of interest. Further, the optimal resource allocation policy (i.e beam and RB) for a given user is also obtained by solving P2[1].

VI. Disjoint User Clustering

In this section, we discuss user clustering utilizing the location information of users. In order to provide network services to users in a given geographical area, we discuss the framework for obtaining disjoint clusters, the optimal number of clusters, and the optimal location of gNBs. The optimization problem (P1) to identify the optimal clustering solution is NP-hard [12]. To address the issue of optimal clustering with reduced computational complexity, we explore the k-means++ [13] algorithm of the unsupervised ML framework [14]. In the k-means++ algorithm, $\mathfrak{K}$ centroids are initialized based on probabilities of the user points being selected as the centroid. Therefore, the set of clusters become $C = \{C_1, C_2, .., C_{\mathfrak{K}}, ..., C_{N_g}\}$, and their corresponding set of centroid is given as $\mu = \{\mu_1, \mu_2, .., \mu_{\mathfrak{K}}, .., \mu_{N_g}\}$. In the initialization process, first, a user location is selected randomly and is considered to be the first centroid. Next, the euclidean distance for each user location from the previously selected centroids is computed. Further, each user is assigned to the closest centroid. After that, the probability of each user being selected as the next centroid is computed using the equation 5. This process is repeated until $\mathfrak{K}$ centroids are computed for initialization. Finally, using this initial $\mathfrak{K}$ centroids, the k-means algorithm [15] is applied over a user set U to identify the $\mathfrak{K}$ disjoint clusters.

$$\mathcal{P}_{u_i} = \frac{\left(d(u_i, \mu_{\mathfrak{K}})\right)^2}{\sum_{u_{\tilde{i}}\in C_{\mathfrak{K}}} \left(d(u_{\tilde{i}}, \mu_{\mathfrak{K}})\right)^2} \tag{5}$$

where, $d(u_i, \mu_{\mathfrak{K}})$ is eucledian distance of user u_i to it's closest centroid $\mu_{\mathfrak{K}}$.

Utilizing the above clustering procedure, we identify the optimal number of gNBs and their optimal locations to provide network services to all the users in the given geographical area A. In this process, optimal cluster centroids are considered to be optimal gNB locations. To identify the optimal number of gNBs (constrained by the maximum number of gNBs available to the network operator), we perform the cluster analysis for all gNBs (i.e, $\mathfrak{K} = 1, 2, ..., N_g$). In this paper, we evaluate the performance of the clustering solution utilizing the Calinski-Harabasz (CH) criteria. Further, we consider S $\left(S = [S_1, S_2, \cdots, S_{\mathfrak{K}}, \cdots, S_{N_g}]\right)$ to be the vector of the performance metric. The average of all cluster centers (i.e. the global cluster center) is denoted by $\bar{\mu}$. Considering $u_i = \{u_{ix}, u_{iy}\}$ and $u_{\tilde{i}} = \{u_{\tilde{i}x}, u_{\tilde{i}y}\}$ as two sample points from the user set; the Euclidean distance between them is given as

$$d\left(u_i, u_{\tilde{i}}\right) = \|u_i - u_{\tilde{i}}\| = \sqrt{\left(u_{ix} - u_{\tilde{i}x}\right)^2 \left(u_{iy} - u_{\tilde{i}y}\right)^2} \tag{6}$$

N_q be the number of samples in the cluster C_q $(q = 1, 2, \cdots, \mathfrak{K})$. The inter-cluster variance $B\left(\mathfrak{K}\right)$ is defined as

$$B\left(\mathfrak{K}\right) = \frac{1}{\mathfrak{K} - 1} \sum_{q=1}^{\mathfrak{K}} N_q \left(d\left(\mu_q, \bar{\mu}\right)^2\right) \tag{7}$$

The inter-cluster variance signifies the underlying distribution of cluster centers in real euclidian space. The larger value of inter-cluster variance indicates a better quality of clustering (i.e

[1]The detailed mathematical framework for ILP optimization (P2) is presented in section IX

better separation between disjoint clusters). The compactness $W(\mathfrak{K})$ within the cluster is defined as

$$\mathrm{W}(\mathfrak{K}) = \frac{1}{N_u - \mathfrak{K}} \sum_{q=1}^{\mathfrak{K}} \sum_{\forall u_i \in C_q} (d(u_i, \mu_q))^2. \quad (8)$$

The computed value of $W(\mathfrak{K})$ is used to evaluate the compactness of the cluster (i.e. better cohesion among points belonging to the same cluster). The smaller the value of $W(\mathfrak{K})$ signifies the more compact clusters. The CH index is a combination of $B(\mathfrak{K})$ and $W(\mathfrak{K})$ given as,

$$\mathrm{S}(\mathfrak{K}) = \frac{B(\mathfrak{K})}{W(\mathfrak{K})} = \frac{N_u - \mathfrak{K}}{\mathfrak{K} - 1} \cdot \frac{\sum_{q=1}^{\mathfrak{K}} N_q (d(\mu_q, \bar{\mu}))^2}{\sum_{q=1}^{\mathfrak{K}} \sum_{\forall u_{i \in C_q}} (d(u_i, \mu_q))^2}. \quad (9)$$

The performance of the clustering solution is evaluated by calculating $S(\mathfrak{K}), \forall \mathfrak{K} = 1, 2, .., N_g$. The maximum value of $S(\mathfrak{K})$ results in the optimal number of clusters, thereby the optimal number of gNBs (N_g^*).

$$N_g^* = \arg\max_{\mathfrak{K}} \{S\} \quad (10)$$

The flowchart in Figure 3 illustrates the computation of the optimal number of gNBs.

VII. 3D Beamforming and Antenna Pattern computation, and Sector Extraction

In this section, we discuss the framework of 3D beamforming to direct multiple beams from a gNB along different angular directions. For this purpose, we first discuss the antenna array geometry, next we present a mathematical framework for the computation of beamforming vectors to direct beams in different angular directions. Further, we discuss the methodology to uniquely assign users in different sectors of a given gNB (or cluster).

A. Computation of Beamforming Vector for Simultaneous Beams Generation

We consider that a gNB (with three UPAs) is located at each optimal cluster centroid (obtained previously in the section VI). We consider that each UPA of the gNB serves a non-overlapping sector of 120°. This scheme of 3D beamforming ensures that all the users associated with a particular cluster are provided with network services without co-sector interference. Figure 4 illustrates the UPA geometry for the computation of the beamforming vector. Here, we consider a $N_x \times N_y$ dimensional UPA such that there are N_x and N_y elements along the x and y axis respectively in the local coordinate system of the UPA. The inter-element spacing along the x and y axes is d_x and d_y respectively.

We utilize the 3GPP model [16] of antenna patterns for 3D beamforming. In this respect, the 3D pattern of the single antenna element is given as,

$$A_E(\theta, \phi) = -min\left\{ -\left[A_{E,H}(\phi) + A_{E,V}(\theta) \right], A_{max} \right\} \quad (11)$$

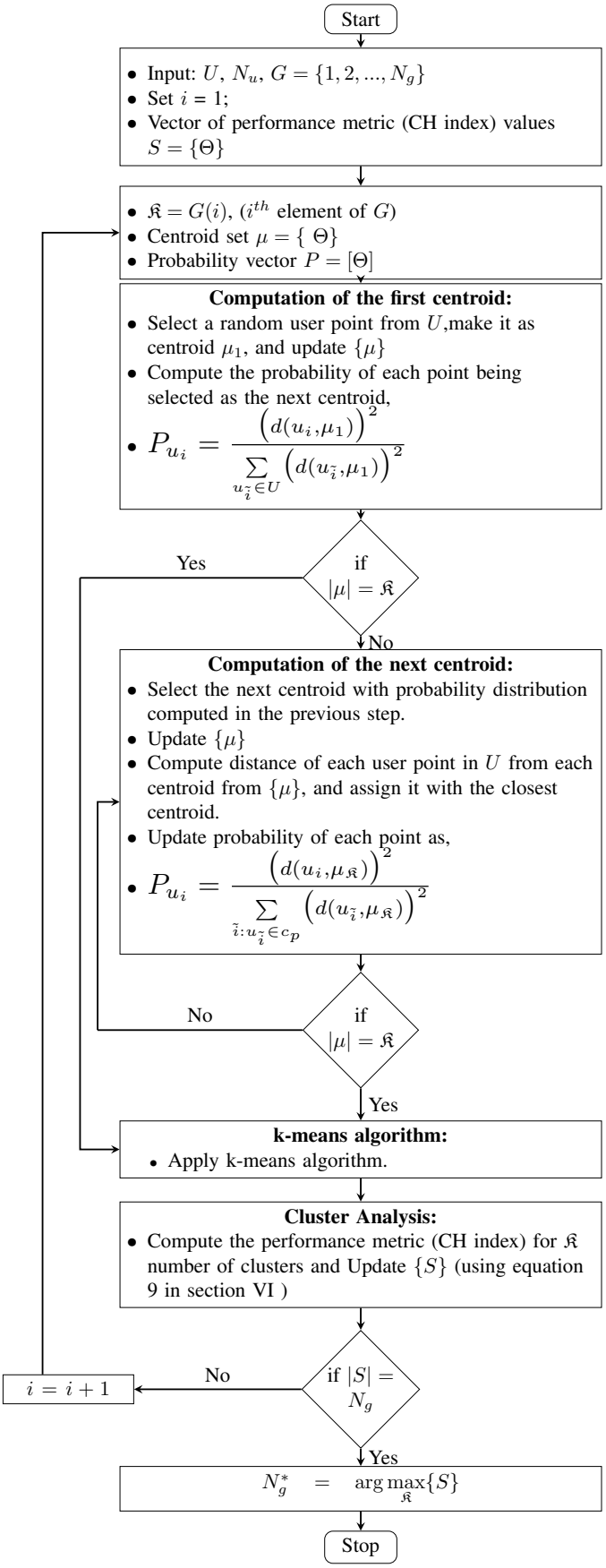

Fig. 3: Flowchart for computation of the optimal number of gNBs.

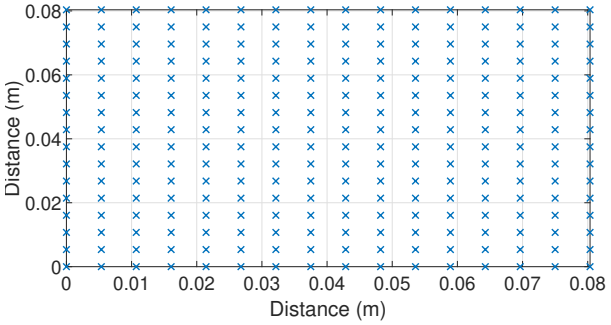

Fig. 4: UPA geometry for the considered operating wavelength. The figure also demonstrates the coordinates of the antenna elements along the local x and y axis of the UPA.

here, $A_{E,H}$ and $A_{E,V}$ are the horizontal and vertical patterns given by equations 12 and 13 respectively. A_{max} is maximum attenuation.

$$A_{E,V}(\theta) = -min\left\{12\left(\frac{\theta-\theta_{tilt}}{\theta_{3dB}}\right)^2, SLA_v\right\} \tag{12}$$

$$A_{E,H}(\phi) = -min\left\{12\left(\frac{\phi}{\phi_{3dB}}\right)^2, A_{max}\right\} \tag{13}$$

Where:

- θ_{3dB} is vertical 3 dB beamwidth.
- ϕ_{3dB} is horizontal 3 dB beamwidth.
- SLA_v side-lobe attenuation in vertical direction.

Each UPA (serving an angular span of 120°) of gNB g_j is generating N_b simultaneous beams. To direct a beam k form gNB j (i.e. b_k^j) in $\left(\theta_0^{j,k}, \phi_0^{j,k}\right)$ direction, the complex excitation ($w_{nx,ny}^{j,k}$) of individual element (nx, ny) is given as,

$$w_{nx,ny}^{j,k} = e^{-j\left[(nx-1)d_x \sin\left(\theta_0^{j,k}\right)\cos\left(\phi_0^{j,k}\right)+(ny-1)d_y \sin\left(\theta_0^{j,k}\right)\sin\left(\phi_0^{j,k}\right)\right]} \tag{14}$$

The complete beamforming vector of beam (b_k^j) in the direction $\left(\theta_0^{j,k}, \phi_0^{j,k}\right)$ is given as,

$$\mathbf{W^{j,k}} = \begin{bmatrix} w_{1,1}^{j,k} & w_{1,2}^{j,k} & \cdots & w_{1,N_y}^{j,k} \\ w_{2,1}^{j,k} & w_{2,2}^{j,k} & \cdots & w_{2,N_y}^{j,k} \\ \cdots & \cdots & & \\ w_{N_x,1}^{j,k} & w_{N_x,2}^{j,k} & \cdots & w_{N_x,N_y}^{j,k} \end{bmatrix}_{N_x \times N_y}. \tag{15}$$

Here, $\mathbf{W^{j,k}}$ is $N_x \times N_y$ matrix.

For simultaneously generating N_b beams from UPA (i.e. in the sector of 120°) of gNB g_j we linearly combine the beamforming vectors $\left(\mathbf{W^{j,k}}\right)$ of the individual beams $b_k^j \forall k = 1, 2, .., N_b$. Therefore, the combined beamforming vector for generation of N_b simultaneous beams is given by equation 16.

$$\mathbf{WC^{N_b}} = \sum_{k=1}^{N_b} \mathbf{W^{j,k}} \tag{16}$$

$\mathbf{WC^{N_b}}$ is $N_x \times N_y$ matrix. Therefore, utilizing equations 15 and 16 the expanded form of $\mathbf{WC^{N_b}}$ is given as,

$$\mathbf{WC^{N_b}} = \begin{bmatrix} \sum_{k=1}^{N_b} w_{1,1}^{j,k} & \sum_{k=1}^{N_b} w_{1,2}^{j,k} & \cdots & \sum_{k=1}^{N_b} w_{1,N_y}^{j,k} \\ \sum_{k=1}^{N_b} w_{2,1}^{j,k} & \sum_{k=1}^{N_b} w_{2,2}^{j,k} & \cdots & \sum_{k=1}^{N_b} w_{2,N_y}^{j,k} \\ \cdots & \cdots & & \\ \sum_{k=1}^{N_b} w_{N_x,1}^{j,k} & \sum_{k=1}^{N_b} w_{N_x,2}^{j,k} & \cdots & \sum_{k=1}^{N_b} w_{N_x,N_y}^{j,k} \end{bmatrix} \tag{17}$$

The array factor of the UPA (serving a sector of 120°) with N_b simultaneous beams is given as,

$$AF(\theta,\phi) = \sum_{nx=1}^{N_x}\sum_{ny=1}^{N_y} \mathbf{WC^{N_b}}(nx,ny) e^{j[(nx-1)\psi_x+(ny-1)\psi_y]}$$

where,

$$\psi_x = kd_x \sin(\theta)\cos(\phi)$$
$$\psi_y = kd_y \sin(\theta)\sin(\phi)$$
$$k = \frac{2\pi}{\lambda_c} \tag{18}$$

In equation 18, $\mathbf{WC^{N_b}}(nx, ny)$ denotes the (nx, ny) element of the matrix $\mathbf{WC^{N_b}}$ and λ_c is the carrier wavelength. The overall gain of a UPA serving the sector of 120° angular span is given in equation 19.

$$G(\theta,\phi) = \left|AF(\theta,\phi)\right|^2 A_E(\theta,\phi) \tag{19}$$

In a similar way, the combined beamforming vector and the corresponding gain are computed for the other two UPAs of gNB g_j. Using the aforementioned framework, we compute the beamforming vector for all gNBs $g_j, \forall j = 1, 2, .., N_g^\star$ present over the geographical area of interest A.

B. Sector extraction

In order to provide wireless network services effectively to all the users associated with a given gNB g_j (or cluster), we divide the entire cluster into 3 non-overlapping sectors. Each sector spans an angular range of 120° in the azimuth plane thereby covering the entire angular range of 360°. As there are N_b beams from each UPA, therefore the angular span of each beam becomes,

$$\theta_{ang} = \frac{120^\circ}{N_b} \tag{20}$$

Corresponding to each cluster $C_{\mathfrak{K}}$ (discussed in section VI), we translate the global coordinates of each user ($u_i \in C_{\mathfrak{K}}$) to the local coordinate system of given cluster $C_{\mathfrak{K}}$. Therefore, the new cluster center is given as,

$$\tilde{\mu}_{\mathfrak{K}} = \mu_{\mathfrak{K}} - \mu_{\mathfrak{K}} \tag{21}$$

and coordinates of the users ($u_i \in C_{\mathfrak{K}}$) are translated using equation 22a and 22b,

$$\tilde{u}_{ix} = u_{ix} - \mu_{\mathfrak{K}x} \quad \forall u_i \in C_{\mathfrak{K}} \tag{22a}$$
$$\tilde{u}_{iy} = u_{iy} - \mu_{\mathfrak{K}y} \quad \forall u_i \in C_{\mathfrak{K}} \tag{22b}$$

Further, we consider the effective radius of the gNB of cluster $C_{\mathfrak{K}}$ as the farthest distance of the user $u_i \in C_{\mathfrak{K}}$. Next, the

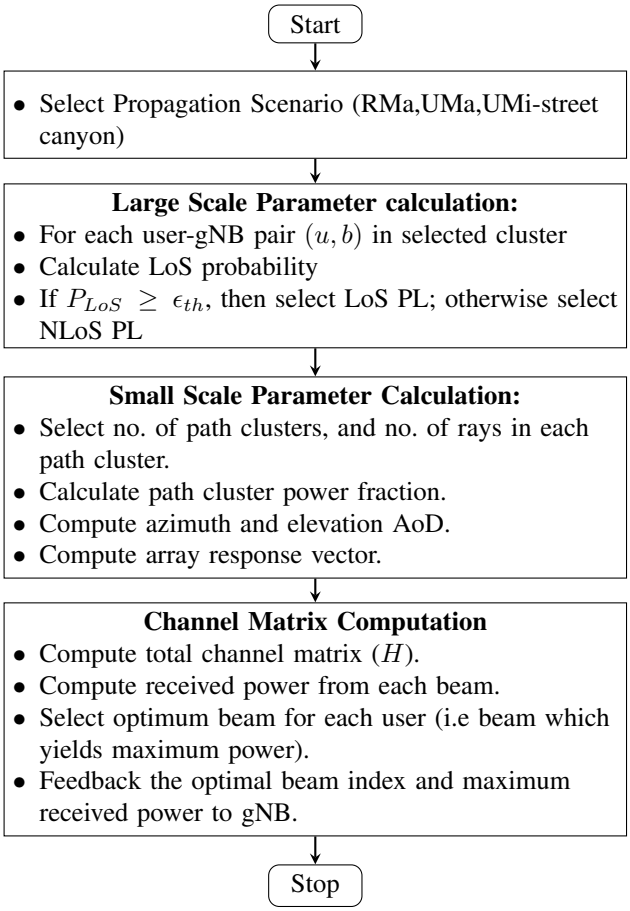

Fig. 5: Flowchart for complete channel matrix computation.

translated cartesian coordinates of the users are converted to spherical coordinates as follows,

$$r^2 = \tilde{u}_{ix}^2 + \tilde{u}_{iy}^2 + \tilde{u}_{iz}^2 \tag{23a}$$

$$\tan(\tilde{\phi}_i) = \frac{\tilde{u}_{iy}}{\tilde{u}_{ix}} \tag{23b}$$

$$\cos(\tilde{\theta}_i) = \frac{\tilde{u}_{iz}}{r} \tag{23c}$$

A user $(u_i \in C_{\aleph})$ is associated with sector 1 of $C_{\aleph}$ if the user's azimuth angle $\tilde{\phi}_i$ is within 0° to 120°. The user is associated with sector 2 if its azimuth angle is within 120° to 240°. Otherwise, a user is associated with sector 3 if its azimuth angle is within 240° to 360°.

VIII. Channel Model and Optimal Beam Computation

For the given 5G network scenario we utilize clustered mmWave channel model along the lines of [16] and [17]. In this work the closed-form expression utilized for power calculation incorporates, PL, shadowing, LoS Probability, beamforming gain, location of users over geographical area A, and small-scale fading effects. The relevant mathematical relations to describe the effects of PL, shadowing and LoS probability are discussed in the following sub-section.

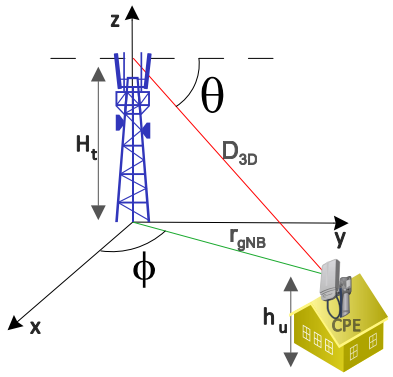

Fig. 6: Beam azimuth and elevation angle at user location.

A. Channel Parameter Computation

1) Large scale fading effects: We consider three outdoor propagation scenarios in 5G viz., RMa, UMa, and UMi-Street Canyon. First, we compute the LoS probability of each user location. The relevant mathematical equations to determine LoS probability of the user for RMa, UMa, and UMi street canyon are presented in the equations 24, 25, and 26 respectively. In equations 24, 25, and 26 r_{gnb} is the two-dimensional distance from gNB. The geometrical representation for computation of the LoS probability is presented in Figure 6. We consider a user to be in the line-of-sight with gNB with due consideration of the propagation scenario, if the LoS probability is greater than a predefined threshold (i.e.ϵ_{th}).

$$P_{rma}^{los} = \begin{cases} 1 \text{ if } r_{gnb} \leq 10m \\ e^{\frac{-\left(r_{gnb}+10\right)}{100}} \text{ if } r_{gnb} > 10m \end{cases} \tag{24}$$

$$P_{uma}^{los} = \begin{cases} 1 \text{ if } r_{gnb} \leq 18m \\ \frac{18}{r_{gnb}} + e^{\left(\frac{-r_{gnb}}{63}\right)} \left(1 - \frac{18}{r_{gnb}}\right) \text{ if } r_{gnb} > 18m \end{cases} \tag{25}$$

$$P_{umi}^{los} = \begin{cases} 1 \text{ if } r_{gnb} \leq 18m \\ \frac{18}{r_{gnb}} + e^{\left(\frac{-r_{gnb}}{36}\right)} \left(1 - \frac{18}{r_{gnb}}\right) \text{ if } r_{gnb} > 18m \end{cases} \tag{26}$$

The relevant PL model is chosen based on the propagation scenario and the computed LoS probability of the user in that propagation scenario. The expressions of PL for RMa, UMa, and UMi street canyon considering the LoS scenario considering the carrier frequency of 28 GHz are derived as in equations 27, 28, and 29 respectively.

$$PL_{rma}^{los} = \begin{cases} 40.684 + 0.013974\sqrt{1122.25 + r_{gnb}^2} + \\ 4.44672 \ln\left(1122.25 + r_{gnb}^2\right) \text{ if } r_{gnb} \leq d_{bp} \\ 17.3718 \ln\left(\sqrt{1122.25 + r_{gnb}^2}\right) + 369.385 \\ \text{if } d_{bp} < r_{gnb} \leq 10\text{Km} \end{cases} \tag{27}$$

$$PL_{uma}^{los} = \begin{cases} 56.9432 + 4.77624 \ln\left(552.25 + r_{gnb}^2\right) \\ \qquad \text{if } r_{gnb} \leq d_{bp} \\ 8.68589 \ln\left(552.25 + r_{gnb}^2\right) - 8.77995 \\ \qquad \text{if } d_{bp} < r_{gnb} \leq 5\text{Km} \end{cases} \quad (28)$$

$$PL_{umi}^{los} = \begin{cases} 61.3432 + 4.566009 \ln\left(72.25 + r_{gnb}^2\right) \\ \qquad \text{if } r_{gnb} \leq d_{bp} \\ 8.68589 \ln\left(72.25 + r_{gnb}^2\right) + 0.0621787 \\ \qquad \text{if } d_{bp} < r_{gnb} \leq 5\text{Km} \end{cases} \quad (29)$$

In a similar way the expressions for the PL with NoLS Table I presents the large-scale parameters for different outdoor propagation scenarios. Further, numerical values of the relevant parameters for different propagation scenarios are utilized from Table I to derive equations 27, 28, and 29 respectively.

TABLE I: Large Scale Channel Parameters

Parameters	**Values**		
Scenario	RMa	UMa	UMi
H_b	35	25	25
h_u	1.5	1.5	1.5
d_{bp}	$2\pi H_b h_u \lambda_c$	$4H_b' h_u' \lambda_c$; $H_b' = H_b - h_E$; $h_h' = h_h - h_E$; $h_E = 1m$	$4H_b' h_u' \lambda_c$; $H_b' = H_b - h_E$; $h_h' = h_h - h_E$; $h_E = 1m$
Shadowing (σ_{SF})	$6dB$(LoS); $8dB$(NLoS)	$4dB$(LoS); $6dB$(NLoS)	$4dB$(LoS); $7.8dB$(NLoS)
ϵ_{th}	0.6	0.6	0.6

2) Small scale fading effects: The scattering effect in mmW channel is modeled by the path clusters. The mmW channel is composed of a random number of path clusters. Each path cluster is characterized by the number of rays, power fraction, azimuth and elevation angle of arrival (AoA), angle of departure (AoD), and angular spread around the central angle of the cluster. The total number of path clusters in a given propagation scenario is denoted by N_p. Further, we consider $\mathcal{M}$ rays in each path cluster p. The power fraction (γ_p) of the p^{th} path cluster is expressed in the following relation,

$$\gamma_p = \frac{\gamma_p'}{\sum_{p=1}^{N_p} \gamma_p'}. \quad (30)$$

Where,

$$\gamma_p' = U_p^{r_\tau - 1} 10^{-0.1 Z_p}, \quad U_p \sim \mathcal{U}[0,1], \quad Z_p \sim \mathcal{N}(0, \zeta^2). \quad (31)$$

In equation 31, r_τ and ζ are constants and treated as model parameters. Further, U_p and Z_p are uniformly and normally distributed random variables respectively. $\mathcal{U}$ denotes the uniform distribution and $\mathcal{N}$ denotes the normal distribution.

For every path cluster (p), the mean azimuth and elevation AoD are given in equations 32 and 33 respectively.

$$\bar{\phi}_{AoD}^p \sim \mathcal{U}[0, 2\pi] \quad \forall p = 1, 2, \cdots, N_p \quad (32)$$

$$\bar{\theta}_{AoD}^p \sim \mathcal{U}[0, 2\pi] \quad \forall p = 1, 2, \cdots, N_p \quad (33)$$

Where, $\bar{\phi}_{AoD}^p$ is mean azimuth AoD for p^{th} path cluster, and $\bar{\theta}_{AoD}^p$ is mean elevation AoD for p^{th} path cluster. For each ray m ($m = 1, 2, \cdots, \mathcal{M}$) in p^{th} path cluster the azimuth AoD is given by

$$\phi_{AoD}^{p,m} \sim \mathcal{N}(\bar{\phi}_{AoD}^p, \sigma_{\phi_{AoD}}^p) \; \forall m = 1, 2, \cdots, \mathcal{M} \quad (34)$$

$\phi_{AoD}^{p,m}$ is the azimuth AoD of the m^{th} ray in the p^{th} path cluster. Here, $\bar{\phi}_{AoD}^p$ is given by equation 32. $\sigma_{\phi_{AoD}}^p$ is an exponentially distributed random variable with mean $\lambda_{\phi_{AoD}}^p$ for p^{th} path cluster. Since we consider single antenna users therefore we do not consider AoA at the receiver antenna array. Similarly, For each ray m ($m = 1, 2, \cdots, \mathcal{M}$) in p^{th} path cluster the elevation AoD is given by

$$\theta_{AoD}^{p,m} \sim \mathcal{N}(\bar{\theta}_{AoD}^p, \sigma_{\theta_{AoD}}^p) \; \forall m = 1, 2, \cdots, \mathcal{M} \quad (35)$$

$\theta_{AoD}^{p,m}$is the elevation AoD of the m^{th} ray in the p^{th} path cluster. Here, $\bar{\theta}_{AoD}^p$ is given by equation 33 and $\sigma_{\theta_{AoD}}^p$ is an exponentially distributed random variable with mean $\lambda_{\theta_{AoD}}^p$. The effective channel between a gNB g_j and user u_i is expressed as,

$$\mathbf{H}^{(\mathrm{u_i})} = \sqrt{10^{-(P_L + \mathcal{X}_\sigma)/10}} \times G(\theta, \phi) \times \left(\sum_{p=1}^{N_p} \sum_{m=1}^{\mathcal{M}} g_{p,m} u_{tx}(\phi_{AoD}^{p,m}, \theta_{AoD}^{p,m}) \right). \quad (36)$$

In equation (36) $\mathcal{X}_\sigma$ is the lognormally distributed random variable with variance σ_{SF}. $g_{p,m}$ is the complex small scale fading gain on the m^{th} ray of p^{th} path cluster. The mathematical expression of $g_{p,m}$ is given as,

$$\bar{g}_{p,m} \sim \mathcal{CN}(0, \gamma_p 10^{-0.1 PL}) \quad (37)$$

where, $\mathcal{CN}$ denotes the complex normal distribution. P_L is the PL depending upon the propagation scenario (RMa, UMa, and UMi Street-Canyon) and LoS condition. The relevant PL expression is substituted in equation (37) utilizing equations (24, 25, 26, 27, 28, 29). u_{tx} is the array response vector of transmitter side UPA to the AoDs. u_{tx} is expressed as,

$$\mathbf{u}_{tx}(\phi_{AoD}^{p,m}, \theta_{AoD}^{p,m}) = \mathbf{a}_{\mathrm{N_x}}(\theta) \otimes \mathbf{a}_{\mathrm{N_y}}(\phi) \in \mathbb{C}^{N_x \times N_y}. \quad (38)$$

$\otimes$ denotes the Kronecker product. The expression for $\mathbf{a}_{\mathrm{N_x}}(\theta)$ and $\mathbf{a}_{\mathrm{N_y}}(\theta)$ are given in equations

$$\mathbf{a}_{\mathrm{Nx}}(\phi_{AoD}^{p,m}, \theta_{AoD}^{p,m}) = \left[1, e^{j\frac{2\pi}{\lambda_c} d_x (\sin(\theta_{AoD}^{p,m}) \cos(\phi_{AoD}^{p,m}))} \cdots e^{j\frac{2\pi}{\lambda_c} d_x ((N_x - 1) \sin(\theta_{AoD}^{p,m}) \cos(\phi_{AoD}^{p,m})))}\right] \quad (39)$$

$$\mathbf{a}_{\mathrm{Ny}}(\phi_{AoD}^{p,m}, \theta_{AoD}^{p,m}) = \left[1, e^{j\frac{2\pi}{\lambda_c} d_y (\sin(\theta_{AoD}^{p,m}) \sin(\phi_{AoD}^{p,m}))} \cdots e^{j\frac{2\pi}{\lambda_c} d_y ((N_y - 1) \sin(\theta_{AoD}^{p,m}) \sin(\phi_{AoD}^{p,m}))}\right] \quad (40)$$

The received power $\left(p_{u_i, g_j, b_k}^{(\mathrm{r})}\right)$ at user u_i from gNB g_j using beam b_k is given as,

$$p_{u_i, g_j, b_k}^{(\mathrm{r})} = \left\| \mathbf{H}^{(\mathrm{u_i})} \mathbf{W}^{\mathbf{j,k}} \right\|_F^2 \quad (41)$$

$\|\cdot\|_F$ denotes the Frobenius norm. The Table II represents the small-scale parameters for different propagation scenarios.

Algorithm 1 Proposed methodology for optimal beam selection

Require: Optimal location of gNbs, Clustering solution (Problem P1)

Ensure: Optimal beam association with the user

Convert the global coordinate of each user $u_i \in C_{\mathfrak{K}}$ to the local coordinate of $C_{\mathfrak{K}}$ (given by equation 22a and 22b).
for $\mathfrak{K} \leftarrow 1, N_g^*$ **do**
    Convert the global coordinate of each user $u_i \in C_{\mathfrak{K}}$ to the local coordinate of $C_{\mathfrak{K}}$ (given by equation 22a and 22b).
    Calculate the distance $d(\tilde{u_i}, \tilde{\mu_{\mathfrak{K}}})$ of each user from the gNB
    The effective coverage radius R_{eff} of the gNB is the distance of the farthest user $u_i \in C_{\mathfrak{K}}$.
    Convert the local cartesian coordinate system of the users $(u_i \in C_{\mathfrak{K}})$ from the previous step to spherical coordinates $\left(r, \tilde{\theta}_i, \tilde{\phi}_i\right)$
    for $u \leftarrow 1, N_{\mathfrak{K}}$ **do**
        for $j \leftarrow 1, 3$ **do**
            if $r \leq R_{eff}$ && $0^\circ \leq \tilde{\phi}_i \leq 120^\circ$ **then**
                User u is associated with sector 1
            else if $r \leq R_{eff}$ && $120^\circ < \tilde{\phi}_i \leq 240^\circ$ **then**
                User u is associated with sector 2
            else if $r \leq R_{eff}$ && $240^\circ < \tilde{\phi}_i \leq 360^\circ$ **then**
                User u is associated with sector 3
            end if
            for $b \leftarrow 1, N_b$ **do**
                Calculate $p^{(\mathrm{r})}_{u_i, g_j, b_k}$
                Calculate $b^*_{u_i} = \arg\max_{b^k}(P^r_{u_i, g_j, b_k})$.
            end for
        end for
    end for
end for

We consider that all subcarriers in an RB experience the same channel condition [18]. The SINR Γ_{u_i, g_j, b_k} with reference to the user u_i and with its associated gNB b_j (i.e., (u_i,b_j)), over beam k is calculated as,

$$\Gamma_{u_i, g_j, b_k^j} = \frac{p_{u_i, g_j, b_k^j}}{\sum\limits_{\substack{b_{k'}^j \in g_j \\ b_{k'}^j \neq b_k^j}} p_{u_i, g_j, b_{k'}^j} + \sigma^2} \tag{42}$$

TABLE II: Small Scale Channel Parameters

Parameters	**Values**		
Scenario	RMa	UMa	UMi
N_p	10(LoS); 11(NLoS)	12(LoS); 20(NLoS)	12(LoS); 19(NLoS)
$\mathcal{M}$	20	20	20
r_τ	3.8(LoS); 1.7(NLoS)	2.5(LoS); 2.3(NLoS)	3(LoS); 2.1(NLoS)
ζ	3	3	3
$\sigma^p_{\phi_{AoD}}$	10.2	10.2	10.2
$\sigma^p_{\theta_{AoD}}$	0	0	0

B. User Association

A user is considered to be associated with beam k of a gNB j which provides the highest SINR. With reference to SINR Γ_{u_i, g_j, b_k^j}, we use the relation $[\alpha, \Phi(\alpha)] = f(\gamma_{u_i, g_j, b_k^j})$, where $f(\Gamma_{u_i, g_j, b_k^j})$ is a function to map the SINR to its corresponding MCS class (i.e., $\alpha, \alpha \in \mathcal{A}$) and bits per symbol $\Phi(\alpha)$ [19]. Considering $\mathcal{B}_{u_i}$ (in bps) to be the data rate demand of user u_i, the number of RBs ($N_{u_i,\alpha}$) required to satisfy the user's data rate demand for MCS class α may be calculated as,

$$N_{u_i,\alpha} = \lceil \frac{\mathcal{B}_{u_i}}{\nu \times \Phi(\alpha)} \rceil \tag{43}$$

where, ν represents the number of symbols per RB [18].

IX. Optimization Framework

In the optimization framework, we aim to design a cost-efficient FiWi access network while satisfying the users' data rate demand. We consider predefined locations for OLT, users, candidate PPSs, and candidate SPSs. We obtained the optimal number of gNBs and their corresponding location for a given simulation scenario using the k-means++ algorithm (section VI). The proposed optimization framework offers details of FiWi network design, including the selection of PS's locations (out of the candidate locations of PPS and SPS), interconnection of all network devices, connectivity of users through fiber/wireless mode, and beam index for the wireless users. Next, we apply the minimum spanning tree (MST) algorithm [20], [21] over the optimization solution to incorporate the sharing of trenching and duct costs. We consider all gNBs transmit with the maximum power over all their RBs, i.e., $P_{b,z,k} = P^{max}_{b,z,k}$ $\forall b \in B$, $z \in Z$, and $k \in K$, where $P^{max}_{b,z,k}$ represents the maximum transmit power of BS b for beam z over RB k.

Step 1 (RSRP Calculation and Candidate MCS Selection): For each user-BS ordered pair (u, b), and for each beam z, we compute RSRP $\gamma_{u,b,z,k}$ considering transmit power $P_{b,z,k}$ using (41). The RSRP value is computed over a single resource element (i.e. over $15kHz$ with numerology 1). The SNR can be computed as follows,

$$SNR = \frac{RSRP}{P_{nre}} \tag{44}$$

where P_nre is noise power over a resource element. In a similar way, the SNR calculation can be extended to the RB as well. We assume that same SNR is experienced by a user over all RBs in a beam z. For (u, b) pair and beam z, MCS m is selected only if block error rate $(BLER) \leq 10\%$, i.e., the SNR experienced by the user over the RB should be greater than the threshold SNR ($\gamma_{th}(m)$) with reference to MCS m [19], [22]. For selected MCS, the number of RBs needed (i.e., $N_{u,m}$) is calculated using (43).

Step 2 (CapEx Optimization using ILP Model and MST): We use the following parameters as input to the ILP model: power transmission matrix $[P_{b,z,k}]$, RB requirement matrix $[N_{u,m}]$, number of RB per beam, set of candidate PPS (S), set of candidate SPS (T), Manhattan distance matrices $\{[D_{u,t}]$ $\forall u \in U, t \in T$, $[D_{u,s}]$ $\forall u \in U, s \in S$, $[D_{b,t}]$ $\forall b \in B, t \in T$, $[D_{b,s}]$ $\forall b \in B, s \in S$, $[D_{t,s}]$ $\forall t \in T, s \in S$, $[D_s]$ between PPS

s ($\forall s \in S$) and OLT}, deployment cost of fiber per km (C_f), cost of an OLT line card (C_o), cost of a PS (C_s), PS splitting ratio (I), line rate of fiber (L_f), and data rate demand of user u (B_u). We also use a large number L ($L \gg |K|$). The ILP model provides intricate details of the designed network, such as the interconnection of all devices, mode (fiber/wireless) selection for a user connection, and usage of RB and MCS. The ILP model is presented in the following: **Variables:**

- $F_u = 1$ if u is fiber user; 0 otherwise.
- $U_u = 1$ if u is wireless user; 0 otherwise.
- $X_s = 1$ if PPS s is connected to OLT; 0 otherwise.
- $Q_t = 1$ if SPS t is present; 0 otherwise.
- $Y_{t,s} = 1$ if SPS t is connected to PPS s; 0 otherwise.
- $A_{u,s} = 1$ if user u is connected to PPS s; 0 otherwise.
- $B_{u,t} = 1$ if user u is connected to SPS t; 0 otherwise.
- $G_{b,s} = 1$ if BS b is connected to PPS s; 0 otherwise.
- $H_{b,t} = 1$ if BS b is connected to SPS t; 0 otherwise.
- $W_{u,b} = 1$ if user u is connected to BS b; 0 otherwise.
- $V_{u,b,z,m} = \begin{cases} 1 \text{ if user } u \text{ is connected to BS } b \\ \quad m \text{ and beam } z \text{ with MCS ; 0 otherwise.} \end{cases}$
- $R_{u,b,z,k,m} = \begin{cases} 1 \text{ if user } u \text{ is connected to BS } b \text{ with} \\ \quad \text{beam } z\text{,RB } k \text{ and MCS } m\text{; 0 otherwise.} \end{cases}$

We define the objective function and the set of constraints in the following.

Minimize,

$$\Bigg(\sum_{s\in S} X_s D_s + \sum_{s\in S}\sum_{t\in T} Y_{t,s} D_{t,s} + \sum_{s\in S}\sum_{u\in U} A_{u,s} D_{u,s} + \sum_{t\in T}\sum_{u\in U} B_{u,t} D_{u,t} + \sum_{b\in B}\sum_{s\in S} G_{b,s} D_{b,s} + \sum_{b\in B}\sum_{t\in T} H_{b,t} D_{b,t}\Bigg) C_f + \sum_{s\in S} X_s (C_o + C_s) + \sum_{t\in T} Q_t C_s \tag{45}$$

Subject to,

$$F_u + U_u = 1 \qquad \forall u \in U \tag{46}$$

$$\sum_{s\in S} A_{u,s} + \sum_{t\in T} B_{u,t} = F_u \qquad \forall u \in U \tag{47}$$

$$\sum_{b\in B} W_{u,b} = U_u \qquad \forall u \in U \tag{48}$$

$$\sum_{z\in Z} J_{u,b,z} = W_{u,b} \qquad \forall u \in U, b \in B \tag{49}$$

$$\sum_{k\in K} R_{u,b,z,k} = N_{u,m} J_{u,b,z} \qquad \forall u \in U, b \in B, z \in Z \tag{50}$$

We aim to minimize the overall CapEx due to fiber deployment, OLT line card and PS cost (45). (46) states that a user is provided either the wireless or the fiber connection. (47) states that a fiber user is connected to either a PPS or an SPS. (48) states that a wireless user is always connected to one BS. (49) ensures that a wireless user is connected to only one beam. (50) ensures that, for a given MCS, the number of RBs allocated to a user must be equal to the number of RBs required by the user.

$$\sum_{u\in U} B_{u,t} + \sum_{b\in B} H_{b,t} \le L Q_t \qquad \forall t \in T \tag{51}$$

$$\sum_{u\in U} B_{u,t} + \sum_{b\in B} H_{b,t} \ge Q_t \qquad \forall t \in T \tag{52}$$

$$\sum_{s\in S} Y_{t,s} = Q_t \qquad \forall t \in T \tag{53}$$

(51,52) state that, in case a user or (and) a BS is required to be connected to a SPS, the SPS must be present. (53) states that, in case a SPS is present, it must be connected to only one PPS.

$$\sum_{u\in U} A_{u,s} + \sum_{t\in T} Y_{t,s} + \sum_{b\in B} G_{b,s} \le L X_s \qquad \forall s \in S \tag{54}$$

$$\sum_{u\in U} A_{u,s} + \sum_{t\in T} Y_{t,s} + \sum_{b\in B} G_{b,s} \ge X_s \qquad \forall s \in S \tag{55}$$

$$\sum_{s\in S} G_{b,s} + \sum_{t\in T} H_{b,t} = 1 \qquad \forall b \in B \tag{56}$$

(54,55) state that, in case a user or (and) a SPS or (and) a BS is required to be connected to a PPS, the PPS must be present. (56) ensures that, a BS is connected to any one PS.

$$\sum_{u\in U} A_{u,s} + \sum_{t\in T} Y_{t,s} + \sum_{b\in B} G_{b,s} \le I \qquad \forall s \in S \tag{57}$$

$$\sum_{u\in U} B_{u,t} + \sum_{b\in B} H_{b,t} \le I \qquad \forall t \in T \tag{58}$$

(57,58) ensure that the number of output connections through a PPS and a SPS is limited by its splitting ratio, respectively.

$$\sum_{k\in K} N_{u,m} J_{u,b,z} \le |K| \qquad \forall u \in U, b \in B, z \in Z \tag{59}$$

$$\sum_{u\in U} R_{u,b,z,k} \le 1 \qquad \forall b \in B, z \in Z, k \in K \tag{60}$$

(59) states that the number of allocated RBs to users by a BS must not be more than the maximum number of available RBs per beam. (60) states that a RB of a BS is allocated to only one user.

$$L_f F_u + \sum_{b\in B}\sum_{z\in Z} N_{u,m} \nu \theta(m) J_{u,b,z} \ge B_u \forall u \in U \tag{61}$$

$$\sum_{u\in U} B_u \le L_f \tag{62}$$

(61) ensures that, the data rate demand of a user should be satisfied either through fiber or wireless connection. (62) states that, the data rate demand of all users should not violate network (fiber) capacity. To consider the sharing of trenching and duct cost, we apply MST algorithm [20], [21] over the ILP output (interconnection of OLT, PPSs, SPSs and ONUs), and obtain the actual fiber layout and CapEx.

X. Simulation Results and Discussions

We consider the rectangular area of 2km×2km wherein users have to be provided network services. With regard to a realistic network scenario, we consider that all users are uniformly distributed. Figure 7(a) illustrates, the fixed location of

TABLE III: Simulation Parameters

Parameters	Values
# cand. PPS, cand. SPS	6, 6
# of RB per beam	500
Max transmit power of BS (P_{max})	30dBm
Gaussian noise figure	-174dBm/Hz
PON standard	Symmetric 10G TDM-PON
Fiber line rate (L_f)	10Gbps
PS splitting ratio (I)	1:64
User data rate demand (B_u)	DR-1 = [2Mbps-12Mbps], DR-2 = [3Mbps-13Mbps], DR-3 = [4Mbps-14Mbps]
Cost of an OLT line card (C_o)	24000$
Cost of a PS (C_s)	70$

OLT and fixed candidate locations for PPSs and SPSs. Figure 7(b) illustrates, the locations of 500 users in the deployment area of 2km×2km. Figure 8 illustrates the optimal number of gNBs (N_g^*) obtained by evaluating the performance of the clustering solution provided by the $k-means++$ algorithm. From Figure 8, we observe that the optimal number of clusters (or gNBs) is 29 for 500 users. Further, Table [] presents the performance evaluation metric obtained for different clusterin solutions by using CH criteria. Figure 9(a) illustrates the optimal location of gNBs in the simulated deployment scenario, whereas, Figure 9(b) illustrates the deployment of the optimal number of gNBs and association of 500 users to different gNB in the deployment area. Table III illustrates the important simulation parameters.

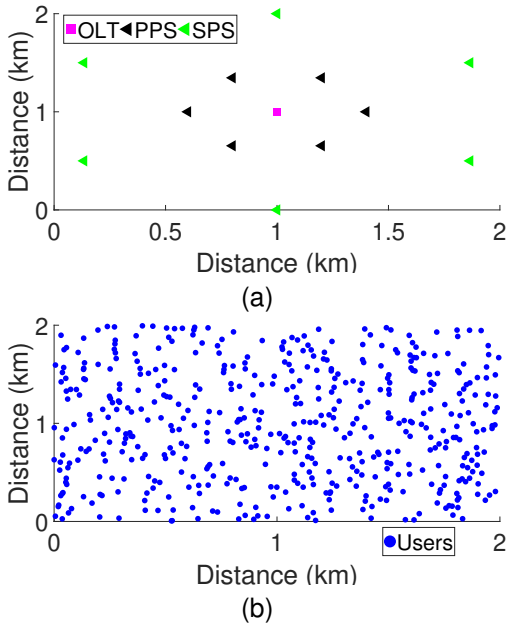

Fig. 7: An illustration of the deployment scenario in $2KM \times 2KM$ rectangular geographical area, (a) the location of optical devices, (b) the locations of 500 users.

Figure 10 illustrates the LoS probability plot obtained by utilizing 3GPP standard for different propagation scenarios. Figure 11 illustrates the curves of PL for RMa, UMa, UMi Street-canyon propagation scenarios. Figures 12(a) and 12(b) illustrate the linear and polar antenna radiation pattern of a

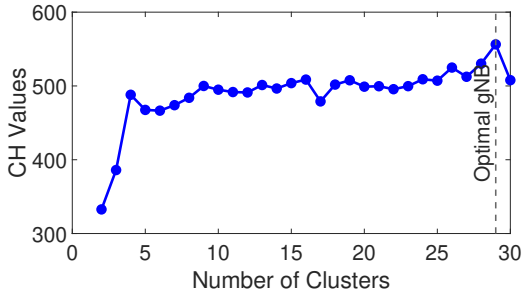

Fig. 8: Performance evaluation of clustering solutions. The performance is evaluated for all gNBs and the optimal number of gNBs is obtained from plot (i.e. maximum CH value)

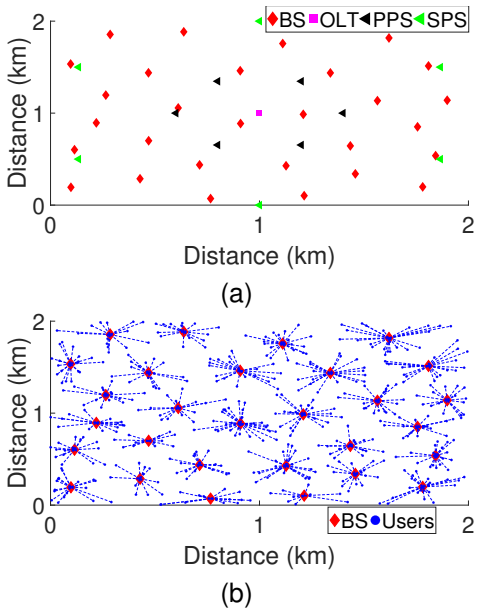

Fig. 9: An illustration of the deployment scenario in $2KM \times 2KM$ rectangular geographical area, (a) the locations of BS (number of BS are computed using $k-means++$ algorithm) along with optical device locations, and (b) the users which are under the coverage area of a BS.

single antenna element in accordance with 3GPP standard. Figures 13(a) and 13(b) illustrate the array factor of given UPA in the linear and polar axis. Figures 14(a) and 14(b) illustrate the radiation pattern of given UPA in polar and linear axis. As observed from Figures 12(a) 13(a) and 12(b) 13(b) the radiation pattern of UPA is obtained by multiplying the radiation pattern of a single element with the array factor of UPA. The complete radiation pattern of a gNB with 24 ($3N_b$) simultaneous beams (using three UPAs) is presented in Figures 15(a) and 15(b).

Figure 16(a) illustrates the locations of the users associated with the first cluster (or gNB) in the global coordinates system. Figure 16(b) illustrates the users and gNB location of the first cluster in a local coordinate system with respect to the gNB. Figure 16(c) illustrates a polar plot of the users' association to the different sectors of the gNB.

Figures 17, 18 and 19 illustrate the CapEx required for the

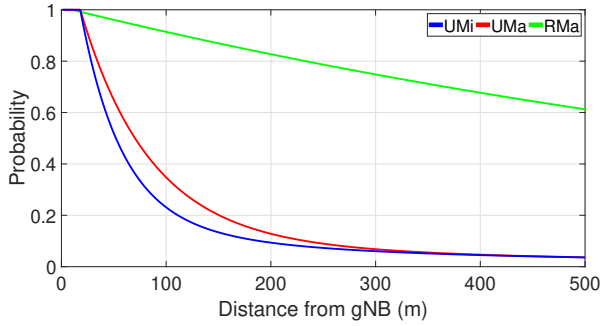

Fig. 10: Line of sight probability for 3GPP 5G RMa, UMa and UMi-street canyon propagation scenarios.

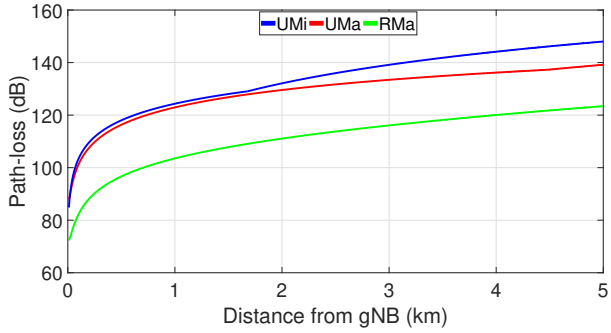

Fig. 11: PL for 3GPP 5G RMa, UMa and UMi-street canyon propagation scenarios.

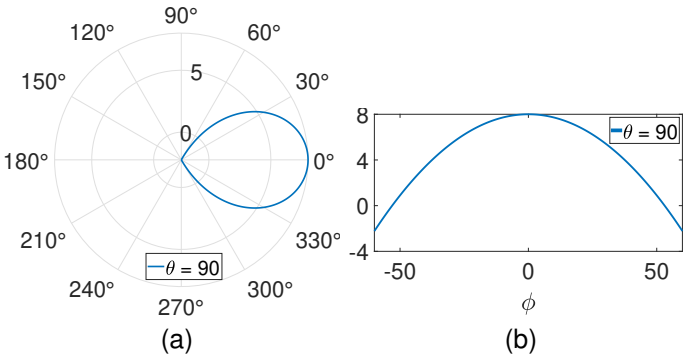

Fig. 12: Radiation pattern of individual antenna element given be 3GPP (a) in the polar plot, (b) in cartesian plot

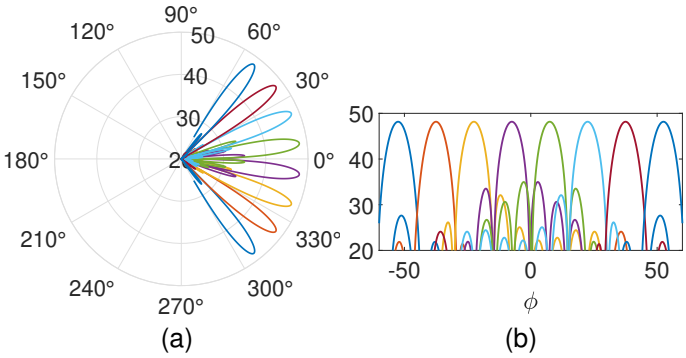

Fig. 13: Radiation pattern of array factor of a 16×16 UPA for generating 8 simultaneous beams (a) in the polar plot, (b)in cartesian plot

deployment of FiWi in RMa, UMa, and UMi Street-Canyon propagation scenarios respectively for different numbers of users and three different data rates profiles. It is observed from Figures 17, 18 and 19 that the CapEx required increases with the increase in the number of users. This trend is observed as the gNBs are unable to provide wireless connectivity to the increased number of users. Further, from Figures 17, 18 and 19 it is observed that with an increase in the average data rate demand of the users (i.e. from DR-1 to DR-3), the CapEx increases. This trend is observed due to the limitation of the RB at the gNBs. Moreover, with the limitation of RBs, gNBs are unable to satisfy the desired QoS of the users (i.e. with high data rate demand). Due to the aforementioned observations, the users which are not accommodated with wireless connections are given fiber connections.

Figure 20 illustrates the comparison of RMa, UMa, and UMi Street-Canyon propagation scenarios for CapEx vs users (with DR-1 data rate profile). As observed from Figure 20 the CapEx requirement for the UMi Street-Canyon propagation scenario is the highest, whereas it is lowest for the RMa. This trend is observed as the propagation losses for the UMi are the highest whereas, it is lowest for RMa (as seen from Figure 11). For the same data rate demand, a wireless user experiences a higher propagation loss thereby, the user is given lower order MCS. Whereas, a user experiencing lower propagation loss is provided with higher-order MCS. Consequently, users in a good propagation environment require fewer RBs, and hence, more users are supported with wireless connections as compared to lossy propagation environment. Figure 21 illustrates the final deployment of FiWi in RMa scenario for 500 users with a DR-1 data rate profile. The red solid line represents the optical fiber connection provided to the users and gNBs through either PPS or SPS whereas, the blue dashed lines represent the wireless connections provided to the users. It can also be observed that the fiber connections are provided through conduit and duct sharing.

XI. Conclusios

We propose TDM-PON and LTE-A based iterative cost-efficient FiWi access network planning strategy. Our method explores suitable FWA/FTTH service mode for users, PSs' locations, and other intricate details of network architecture. We observe that after the second iteration, the CapEx is significantly reduced from that of the first iteration. Even though the CapEx may marginally toggle in the subsequent iterations, the network planning obtained through each iteration is a valid solution satisfying all feasibility constraints and users' QoS requirements. We select the best result out of all the solutions obtained over the iterations. The optimal FiWi access network planning is a complex problem; it is unlikely that the complete problem can be modeled as a single mathematical programming based optimization problem without relaxing the constraints. The network planning being an offline strategy, which is required to be executed only once, before deployment, the proposed ILP based iterative network planning strategy

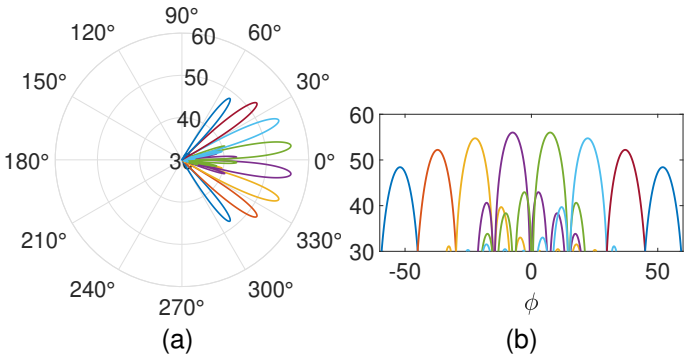

Fig. 14: Radiation pattern of simultaneous 8 beams in one sector (a) in the polar plot, (b)in cartesian plot

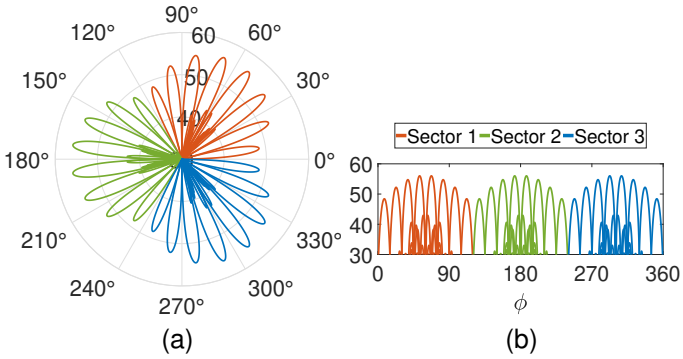

Fig. 15: Radiation pattern of simultaneous 24 beams for three sectors (a) in the polar plot, (b)in cartesian plot

will not pose any challenge for practical usage, specifically in recent times in presence of cloud based computing services.

REFERENCES

[1] Huawei, "4G/5G FWA Broadband White Paper," 2019. [Online]. Available: https://www.huawei.com/en/technology-insights/industry-insights/technology/4g-5g-fwa-broadband-whitepaper.

[2] Samsung, "5G Fixed Wireless Access," 2018. [Online]. Available: https://images.samsung.com/is/content/samsung/assets/global/business/networks/insights/white-paper/samsung-5g-fwa/white-paper_samsung-5g-fixed-wireless-access.pdf.

[3] T. Bose, A. Suresh, O. J. Pandey, L. R. Cenkeramaddi, and R. M. Hegde, "Improving quality-of-service in cluster-based uav-assisted edge networks," *IEEE Transactions on Network and Service Management*, vol. 19, no. 2, pp. 1903–1919, 2022.

[4] S. Kutty and D. Sen, "Beamforming for millimeter wave communications: An inclusive survey," *IEEE communications surveys & tutorials*, vol. 18, no. 2, pp. 949–973, 2015.

[5] Y. P. Zhang and D. Liu, "Antenna-on-chip and antenna-in-package solutions to highly integrated millimeter-wave devices for wireless communications," *IEEE transactions on antennas and propagation*, vol. 57, no. 10, pp. 2830–2841, 2009.

[6] B. P. Rimal, D. Pham Van, and M. Maier, "Mobile-Edge Computing Versus Centralized Cloud Computing Over a Converged FiWi Access Network," *IEEE Trans. Netw. Service Manag*, vol. 14, no. 3, pp. 498–513, 2017.

[7] H. Guo and J. Liu, "Collaborative Computation Offloading for Multi-access Edge Computing Over Fiber–Wireless Networks," *IEEE Trans. Wireless Commun.*, vol. 67, no. 5, pp. 4514–4526, 2018.

[8] A. Ebrahimzadeh and M. Maier, "Cooperative Computation Offloading in FiWi Enhanced 4G HetNets Using Self-Organizing MEC," *IEEE Trans. Wireless Commun.*, vol. 19, no. 7, pp. 4480–4493, 2020.

[9] J. Liu, H. Guo, H. Nishiyama, H. Ujikawa, K. Suzuki, and N. Kato, "New Perspectives on Future Smart FiWi Networks: Scalability, Reliability, and Energy Efficiency," *IEEE Commun. Surveys Tuts.*, vol. 18, no. 2, pp. 1045–1072, Secondquarter 2016.

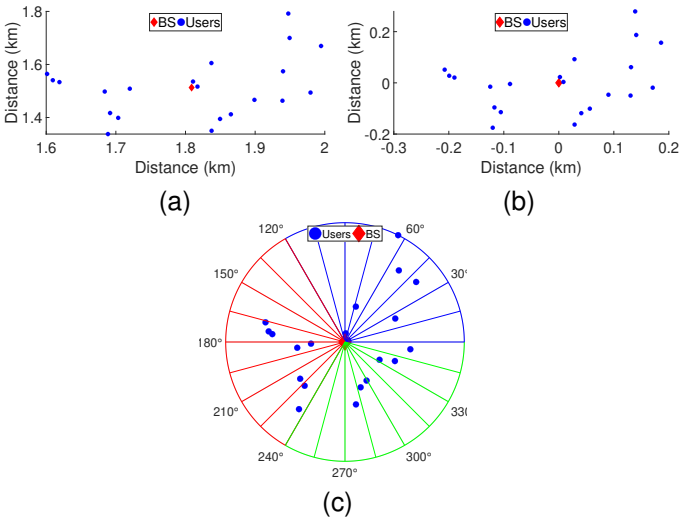

Fig. 16: Illustration of the user's location in a global and local coordinate system. (a) Users' locations and BS location at the centroid of the cluster in a global coordinate system, (b) Users' location in the local coordinate system with respect to BS, (c) Users in different sectors of BS.

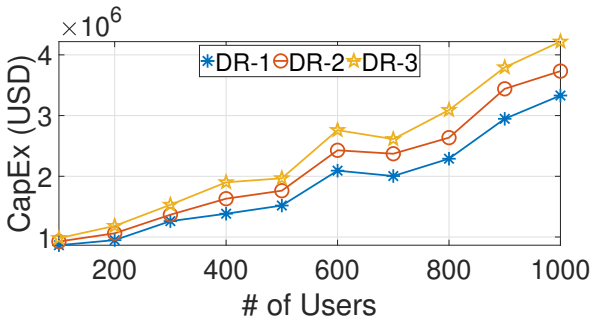

Fig. 17: CapEx in USD for a different number of users for RMA propagation scenario.

[10] 3GPP, "Technical Specification Group Radio Access Network; Study on New Radio (NR) access technology (Rel. 17)," TS 38.912 V17.0.0, Mar. 2022.

[11] M. Giordani, M. Polese, A. Roy, D. Castor, and M. Zorzi, "A tutorial on beam management for 3gpp nr at mmwave frequencies," *IEEE Communications Surveys Tutorials*, vol. 21, no. 1, pp. 173–196, 2019.

[12] D. Aloise, A. Deshpande, P. Hansen, and P. Popat, "Np-hardness of euclidean sum-of-squares clustering," *Machine learning*, vol. 75, no. 2, pp. 245–248, 2009.

[13] D. Arthur and S. Vassilvitskii, "k-means++: The advantages of careful seeding," Stanford, Tech. Rep., 2006.

[14] J. S. Almeida and C. A. Prieto, "Automated unsupervised classification of the sloan digital sky survey stellar spectra using k-means clustering," *The Astrophysical Journal*, vol. 763, no. 1, p. 50, 2013.

[15] A. Likas, N. Vlassis, and J. J. Verbeek, "The global k-means clustering algorithm," *Pattern recognition*, vol. 36, no. 2, pp. 451–461, 2003.

[16] 3GPP, "Technical Specification Group Radio Access Network;Study on channel model for frequency spectrum above 6 GHz (Rel. 15)," TR 38.900 V15.0.0, 2018.

[17] M. R. Akdeniz, Y. Liu, M. K. Samimi, S. Sun, S. Rangan, T. S. Rappaport, and E. Erkip, "Millimeter wave channel modeling and cellular capacity evaluation," *IEEE journal on selected areas in communications*, vol. 32, no. 6, pp. 1164–1179, 2014.

[18] V. J. Kotagi, R. Thakur, S. Mishra, and C. S. R. Murthy, "Breathe to Save Energy: Assigning Downlink Transmit Power and Resource Blocks

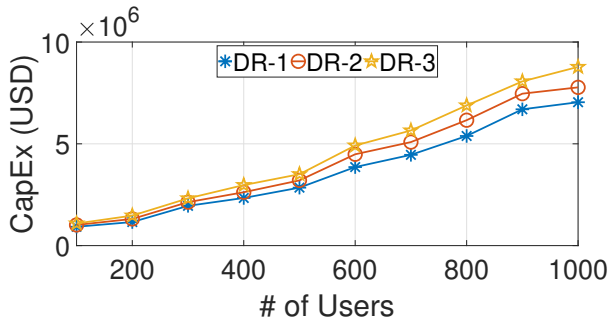

Fig. 18: CapEx in USD for a different number of users for UMA propagation scenario.

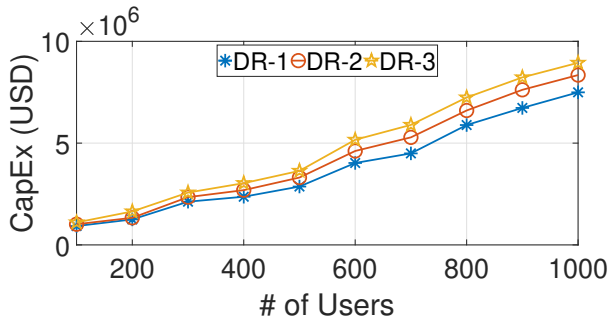

Fig. 19: CapEx in USD for a different number of users for UMA propagation scenario.

to LTE Enabled IoT Networks," *IEEE Commun. Lett.*, vol. 20, no. 8, pp. 1607–1610, Aug. 2016.

[19] 3GPP, "Evolved Universal Terrestrial Radio Access (E-UTRA); Radio Frequency (RF) system scenarios (Rel. 14)," TR 36.942 V14.0.0, Mar. 2017.

[20] H. Chen, Y. Li, S. K. Bose, W. Shao, L. Xiang, Y. Ma, and G. Shen, "Cost-Minimized Design for TWDM-PON-Based 5G Mobile Backhaul Networks," *IEEE J. Opt. Commun. Netw.*, vol. 8, no. 11, pp. B1–B11, 2016.

[21] M. S. Akhtar, P. Biswas, A. Adhya, and S. Majhi, "Cost-efficient Mobile Backhaul Network Design over TWDM-PON," in *2020 IEEE International Conference on Advanced Networks and Telecommunications Systems (ANTS)*, 2020, pp. 1–6.

[22] 3GPP, "Evolved Universal Terrestrial Radio Access (E-UTRA); physical layer procedures (Rel. 14)," TS 36.213 V14.13.0, Dec. 2019.

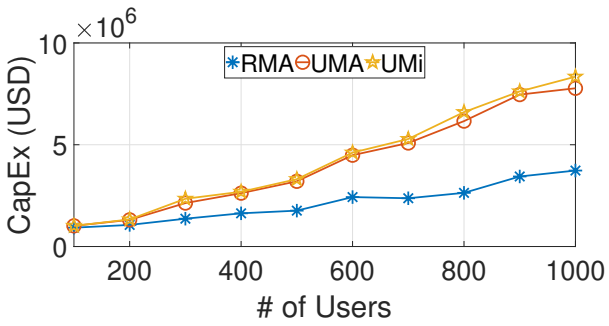

Fig. 20: CapEx comparison for RMA, UMA, and UMi propagation scenario for DR-1 data rate profile.

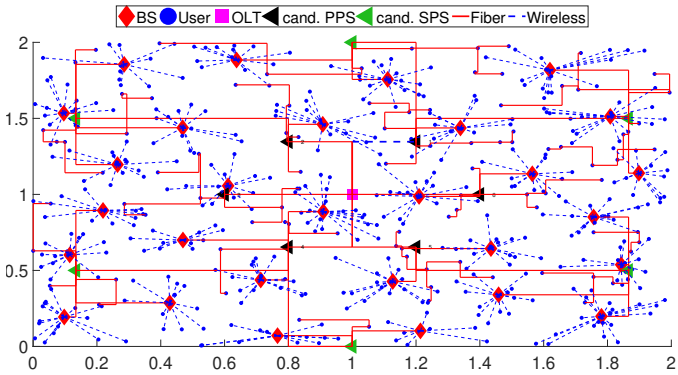

Fig. 21: Deployment of FiWi access network in RMa scenario for 500 users with DR-1 data rate profile.